Analytical Model for the Maximum Radar Cross Section of Dielectric Trihedral Corner Reflectors

Christian Buchberger
Associate Professorship of Microwave Engineering
Technical University of Munich
Munich, Germany
chris.buchberger@tum.de

Thomas Eder
BMW AG
Munich, Germany
Thomas.EG.Eder@bmw.de

Florian Pfeiffer
perisens GmbH
Feldkirchen, Germany
pfeiffer@perisens.de

Erwin Biebl
Associate Professorship of Microwave Engineering
Technical University of Munich
Munich, Germany
biebl@tum.de

***Abstract*—Millimeter wave measurements and simulations of dielectric trihedral corner reflectors are presented. Similar to conventional metallic corner reflectors they exhibit retroreflective properties but show interference effects for perpendicular incidence. This leads to significantly fluctuating values of the radar cross section in dependency of the reflector size and material constants. A mathematical proof is given, showing that the path length through a trihedral is constant for perpendicular incidence. This serves as the basis for deriving an analytical model of the radar cross section to evaluate design parameters for dielectric corner reflectors.**

***Index Terms*—radar cross section, radar measurements, geometrical optics, electromagnetic modeling, millimeter wave propagation, electromagnetic reflection**

I. Introduction

In the radar community, using dielectrics as potential targets for measurement systems or calibration purposes is not very widespread. Models of the radar cross section (RCS) of canonical dielectric objects such as spheres, cylinders or cones have been established very early [1]–[3]. During these times, especially scattering in the Mie and Rayleigh region were of interest, because of the relatively long wavelengths that were used or because of very small objects like raindrops and hail [4]. Later, dielectric bodies of revolution have been studied extensively [5]. Recently, dielectrics have been used in RCS reduction techniques [6], [7]. Concerning radar targets, dielectrics have been investigated as an angular enhancement for metallic retroreflectors [8] and for frequency notch filtering [9] in dihedral corner reflectors. In general, analyses that are either based on electromagnetic scattering or geometrical optics are often limited to numerical results. We propose an approach that, based on the comparison of known radar cross sections in the geometric region, derives an analytical equation of the RCS for arbitrary lossless dielectric trihedral corner reflectors.

In a previous paper [10], we found that just like corner cube reflectors used in optical applications [11], a dielectric trihedral corner reflector can be manufactured that exhibits similar behavior to a conventional metallic one, as long as the dielectric loss factor $\tan\delta$ of the dielectric is small enough. There are nevertheless some major differences concerning the angle dependency of the RCS, especially concerning perpendicular illumination, as it can decrease significantly if the wrong dimensions of the reflector are chosen.

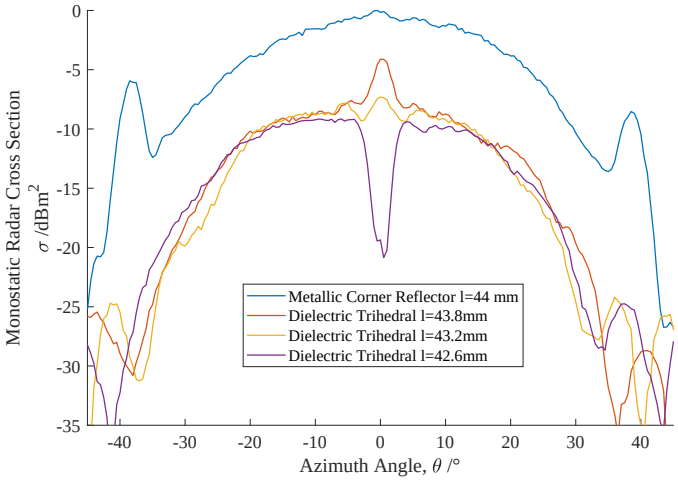

Fig. 1. Radar cross section measurements in the $76-77\,\mathrm{GHz}$ range using a FMCW radar. The blue line represents a metallic corner reflector with a RCS of $1\,\mathrm{m}^2$ as reference. The other lines show the angle dependant azimuthal RCS of dielectric trihedrals with $\epsilon_\mathrm{r}=2.47$ and $\tan\delta=0.005$. For perpendicular illumination at $\theta=0\,^\circ$ they exhibit minima and maxima, suggesting interference.

This paper gives insight on how to determine the design parameters of such a reflector to achieve the desired outcome of the resulting RCS. In Section II, first examples of the interference phenomenon occurring for perpendicular illumination in dielectric trihedral corner reflectors by measurements and simulations are given. To further develop an analytical model of the perpendicular RCS, Section III introduces a mathematical proof of the constant ray length inside the

trihedral for perpendicular incidence. Finally, in addition to deriving the analytical model, Section IV also evaluates the model against computer simulations.

II. Problem Description

A dielectric trihedral corner reflector works on the principle of total internal reflection. For a relatively large angular range, incident rays experience total reflection at the back between the medium and the air and are reflected back to the transmitter. The angular range over which total internal reflection occurs is generally dependent on the relative permittivity ϵ_r. Fig. 1 shows measurement results of the RCS of three different dielectric reflectors versus the azimuth angle. The measurements were made analogous to [10] with the FMCW radar sensor AWR1643BOOST by Texas Instruments [12] in the frequency range of $76-77\,\mathrm{GHz}$. The dielectric reflectors shown in Fig. 2 are manufactured from polyamide-12 using a selective laser sintering process. The dielectric properties were measured analogously to [13].

The measurement results of the three reflectors show some differences compared to the conventional metal reflector. Firstly, it can be seen that the characteristic "bat-ears" are absent at $\theta = \pm 39°$. This is due to the fact that for rising incidence angles, the critical angle at the medium to air boundary is not reached and therefore total internal reflection does not occur. Secondly, the opening angle is smaller, depending on the relative permittivity of the material used. Thirdly, the overall RCS is smaller as well, partly because of the lossy material, partly because of other losses that will be discussed further in Section IV. Most noticeable however, is the large difference in the RCS at $\theta = 0°$. At a constant observation wavelength and using the same material, the traveled path of the wave in the medium changes depending on the size of the reflector. Since there is also a reflection at the first interface between air and medium in addition to the total reflection, it can be assumed that interference occurs between these two wave components. This is also illustrated in Fig. 3. The mean electric field strength is shown for a monochromatic excitation by a plane wave incident to a lossless dielectric trihedral. Both simulations use the same medium, but the dimensions of the reflectors were changed by half the effective wavelength. This results in the corresponding reduction or increase of the mean electric field strength in free space and respectively the total power that is reflected back.

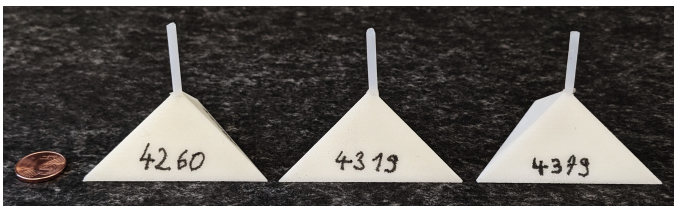

Fig. 2. Three dielectric trihedral corner reflectors of different sizes, (fLTR: $l_1 = 42,6\,\mathrm{mm}, l_2 = 43,2\,\mathrm{mm}, l_3 = 43,8\,\mathrm{mm},$) made of polyamide-12 ($\epsilon_r = 2.47, \tan\delta = 0.007$) and manufactured by selective laser sintering.

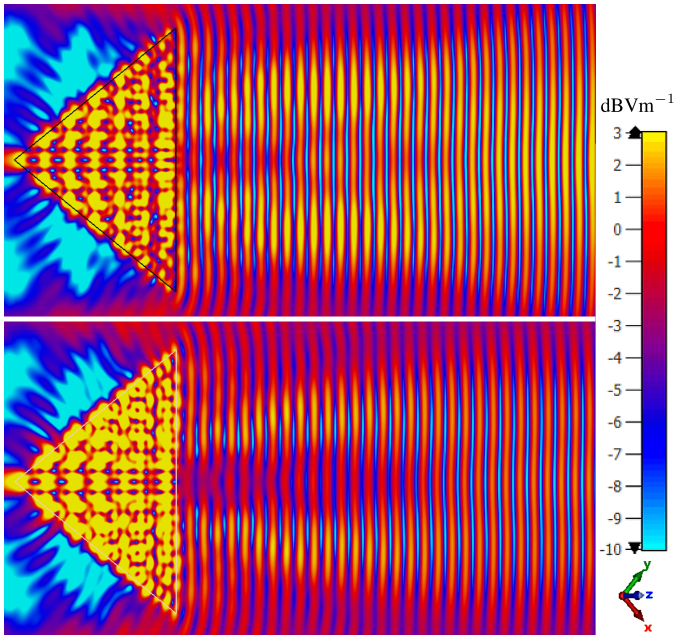

Fig. 3. Average electric field distribution after excitation with a linearly polarized plane wave of two lossless dielectric corner reflectors of different sizes with $\epsilon_r = 2.47$. Top: Constructive interference at the medium interface leads to higher reflected power. Bottom: Less reflected power due to the destructive interference of the reflection at the first interface with the reflection of the trihedral. Both show a loss of power at their tips. CST Simulation, FIT Solver.

To further analyze the interfering behavior of the dielectric trihedral for perpendicular illumination, we show in the following that all paths through the trihedral taken are of equal length. This is done by a geometrical optics approach, using rays as a representation of the incident plane wave.

III. Proof of Constant Ray Length in Trihedral Corner Reflectors

Definition 1. A *trihedral corner reflector* is described by three isosceles, right-angled triangles acting as *reflection surfaces*. In case its reflection surfaces R_{xy}, R_{yz}, and R_{xz} are a subset of the xy-, yz-, and the xz-plane respectively, a trihedral corner reflector width edge length $l \in \mathbb{R}$ is described in terms of

$$R_{xy}(l) = \left\{ r_{xy} \in \mathbb{R}^3 \mid \|r\|_1 \leqslant l \wedge r_{xy}^{(1)}, r_{xy}^{(2)} \geqslant 0 \wedge r_{xy}^{(3)} = 0 \right\}. \quad (1)$$

Analogous to that one can define $R_{yz}(l)$, $R_{xz}(l)$. Moreover, the *plane of incidence* of that corner reflector is the set

$$P_{\text{in}}(l) = \left\{ (x,y,z) \in \mathbb{R}^3 \mid x+y+z = l \wedge x,y,z \geqslant 0 \right\}. \quad (2)$$

Definition 2. A *ray* or a *beam* in direction $v \in \mathbb{R}^3$ passing through point $r \in \mathbb{R}^3$ is a line $b \subseteq \mathbb{R}^3$. For every point $y \in \mathbb{R}^3$ along the beam there exists $t \in \mathbb{R}$ such that $y = r + tv$.

Lemma 3. *Let $R \subseteq \mathbb{R}^3$ be a reflection surface with normal vector $n \in \mathbb{R}$. Let $b_{in} \in \mathbb{R}^3$ be an incident beam in direction $v_{in} \in \mathbb{R}^3$. The directional vector $v_{out} \in \mathbb{R}^3$ of the reflected beam $b_{out} \in \mathbb{R}^3$ is given by $v_{out} = v_{in} - 2(n \cdot v_{in})n$.*

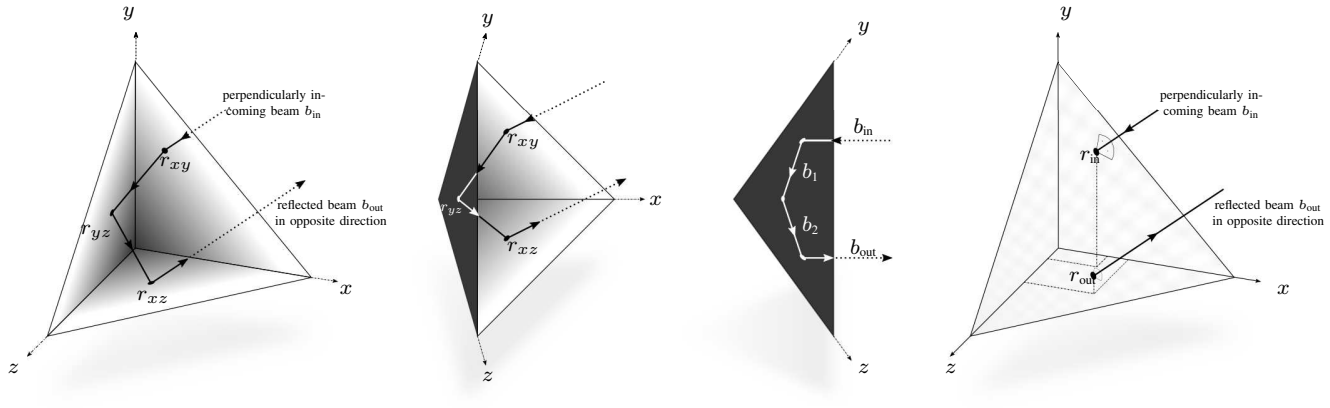

Fig. 4. An exemplary presentation of a trihedral corner reflector and a perpendicularly incoming, threefold reflected beam from three different perspectives. A right-handed coordinate system can always be assigned such that the beams hit points are within the xy-plane, yz-plane, and xz-plane in sequence. To proof theorem 5 it is sufficient to express the point of incidence r_{in}, the exit point r_{out}, and reflection points r_{yz} and r_{xz} as a function of the first reflection point r_{xy}. Calculating the sum of the distances $\overline{r_{\text{in}}r_{xy}}$, and $\overline{r_{xz}r_{\text{oout}}}$, and the length of the beams b_1, b_2 one determines a constant beam length inside the reflector.

Proof. Since all vectors are assumed to be normalized, the following holds

$$\begin{aligned} v_{\text{out}} \cdot n &= (v_{\text{in}} - 2(n \cdot v_{\text{in}})n) \cdot n \\ &= v_{\text{in}} \cdot n - 2(n \cdot v_{\text{in}}) \\ &= -v_{\text{in}} \cdot n. \end{aligned} \tag{3}$$

Hence, the angle of incidence $\theta_{\text{in}} = \pi - \arccos(v_{\text{in}} \cdot n)$ equals the angle of reflection $\theta_{\text{out}} = \arccos(v_{\text{out}} \cdot n)$. Furthermore, since $(v_{in} \times v_{out}) \cdot n = 0$ the beams y_{in} and y_{out} are within the same plane, thus y_{out} fulfills the law of reflection. □

Corollary 4. *Let b_{in} be a beam with direction $v_{in} = (x, y, z)^\intercal$ reflected at the xy-, yz-, or the xz-plane. The direction v_{out} of the reflected beam b_{out} is given by*

$$v_{out} = (x, y, -z)^\intercal, \; v_{out} = (-x, y, z)^\intercal, \; v_{out} = (x, -y, z)^\intercal.$$

Theorem 5. *The length of a perpendicularly incoming beam in a trihedral corner reflector is constant if reflected thrice.*

Proof. Without loss of generality, the perpendicularly incoming beam $b_{\text{in}} \subseteq \mathbb{R}^3$ with normalized direction $v_{\text{in}} = -1/\sqrt{3}\,(1,1,1)^\intercal$ is reflected threefold in sequence at the reflection surfaces R_{xy}, R_{yz} and R_{xz} of a trihedral corner reflector with edge length $l = 1$. The hit points are denoted as r_{xy}, r_{yz}, and r_{xz} (cf. Fig. 4). Since the beam is reflected thrice there are two beams b_1, b_2 completely inside the corner reflector. According to corollary 4, the direction v_1 of beam b_1 is given as $v_1 = -1/\sqrt{3}\,(1,1,-1)^\intercal$. The hit point r_{yz} is the intersection of the reflection surface R_{yz} and beam b_1. By solving the equation

$$\begin{pmatrix} 0 \\ r_{yz}^{(2)} \\ r_{yz}^{(3)} \end{pmatrix} = \begin{pmatrix} r_{xy}^{(1)} \\ r_{xy}^{(2)} \\ 0 \end{pmatrix} - \frac{t}{\sqrt{3}} \begin{pmatrix} 1 \\ 1 \\ -1 \end{pmatrix} \tag{4}$$

in the first coordinate one concludes that $t = \sqrt{3} r_{xy}^{(1)}$ and hence

$$r_{yz} = \left(0, r_{xy}^{(2)} - r_{xy}^{(1)}, r_{xy}^{(1)}\right)^\intercal. \tag{5}$$

Analogously, the third hit point r_{xz} can be written as a function of r_{yz} and hence as a function of r_{xy}, i.e.

$$r_{xz} = \left(r_{xy}^{(2)} - r_{xy}^{(1)}, 0, r_{xy}^{(2)}\right)^\intercal. \tag{6}$$

Finally, the intersections r_{in}, r_{out} of the beams b_{in}, b_{out} with the plane of incidence are given in terms of

$$r_{\text{in}} = -\frac{1}{3} \begin{pmatrix} 1 - 4r_{xy}^{(1)} - r_{xy}^{(2)} \\ 1 - r_{xy}^{(1)} - 4r_{xy}^{(2)} \\ 1 - r_{xy}^{(1)} - r_{xy}^{(2)} \end{pmatrix} \tag{7}$$

and

$$r_{\text{out}} = \frac{1}{3} \begin{pmatrix} 1 + r_{xy}^{(2)} - 2r_{xy}^{(1)} \\ 1 - 2r_{xy}^{(2)} + r_{xy}^{(1)} \\ 1 + r_{xy}^{(2)} + r_{xy}^{(1)} \end{pmatrix}. \tag{8}$$

The length L between all those points is the beam length inside the corner reflector, i.e.

$$\begin{aligned} L &= \overline{r_{\text{in}}r_{xy}} + \overline{r_{xy}r_{yz}} + \overline{r_{yz}r_{xz}} + \overline{r_{xz}r_{\text{out}}} \\ \ldots &= \frac{\sqrt{3}}{3} \Big(1 - r_{xy}^{(1)} - r_{xy}^{(2)} + 3r_{xy}^{(1)} \\ &\quad + 3(r_{xy}^{(2)} - r_{xy}^{(1)}) + 1 - 2r_{xy}^{(2)} + r_{xy}^{(1)}\Big) \\ &= 2\frac{\sqrt{3}}{3}. \end{aligned} \tag{9}$$

Hence, the length of perpendicularly incoming beam in a trihedral corner reflector is constant. □

IV. Analytical Interference Model for Lossless Dielectric Corner Reflectors

As established in Section III, the traveled path of the electromagnetic wave represented by a geometrical ray is constant with length $L = 2\frac{\sqrt{3}}{3}l$, when l is the edge length of the trihedral from the origin along the axes. The interferences shown in Section II can be explained by a superposition of two different waves interfering coherently at the first reflecting surface. Using the height and the relative permittivity of the

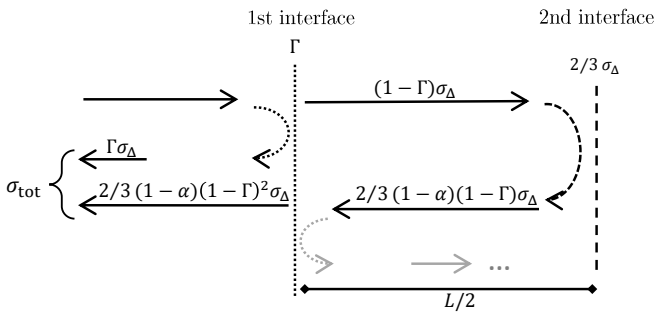

Fig. 5. A two-interface model of the lossless dielectric trihedral. The first interface has a power reflection coefficient Γ and the effective surface area of a equilateral triangle. The second interface only exhibits two-thirds of the first effective surface area and introduces an additional loss factor α.

medium, we can establish a mathematical expression to find constructive and destructive interferences given a certain wavelength. Constructive interferences will occur if the traveled path inside the trihedral, i.e. L, is an integer multiple of the effective wavelength $\lambda_{\text{eff}} = \lambda/\sqrt{\epsilon_{\text{r}}}$. Equivalently, destructive interferences happen for half integer multiples.

A. Derivation of the analytical model

The basic principle of the derivation follows the bodies' reflectance model shown in Fig. 5. The trihedral is divided into two interfaces, the first being a equilateral triangle. The maximum RCS of an equilateral triangle $\sigma_{\triangle}$ with side length of $l\sqrt{2}$ for a perfect electric conductor is given by [14, p.231]

$$\sigma_{\triangle} = \frac{3\pi l^4}{\lambda^2}. \tag{10}$$

For a dielectric equilateral triangle with a relative permittivity ϵ_{r}, power is only partially reflected. As only perpendicular waves are investigated, the power reflection coefficient Γ derived from Fresnel equations [15, p. 207] is

$$\Gamma = \left(\frac{1-\sqrt{\epsilon_r}}{1+\sqrt{\epsilon_r}}\right)^2, \tag{11}$$

independent of the waves' polarization and, consequently, the RCS $\sigma_{\blacktriangle}$ of the first interface of the trihedral corner reflector is

$$\sigma_{\blacktriangle} = \Gamma\sigma_{\triangle}. \tag{12}$$

To find the RCS corresponding to the second interface, we use $(1-\Gamma)\sigma_{\triangle}$ as the maximum RCS possible that could eventually interfere and form the total RCS σ_{tot}. In a lossless dielectric trihedral corner reflector, there are two main factors reducing the effective surface area. Firstly, geometrically only two-thirds of the surface area in comparison to the equilateral triangle is contributing to the RCS. This is also the case for metallic corner reflectors, as the three outer tips do not reflect into the direction of incidence [14, p. 239]. Secondly, in dielectric corner reflectors there seems to be a significant loss of power. Measurements as well as the electric field distribution of the time domain simulations displayed in Fig. 3 show a leakage at the tip of the trihedral. With this loss coefficient α we can give an inner contributing RCS σ_{inner} as

$$\sigma_{\text{inner}} = \frac{2}{3}(1-\alpha)(1-\Gamma)\sigma_{\triangle}. \tag{13}$$

Again, a part of the contributing RCS of σ_{inner} is reflected at the first interface, giving

$$\sigma'_{\text{inner}} = \frac{2}{3}(1-\alpha)(1-\Gamma)^2\sigma_{\triangle}. \tag{14}$$

Only one total inner reflection is considered in the following, as higher order contributions (grey arrow and dots in Fig.5) fall off exponentially and are therefore neglected.

To combine the two outcomes, we propose to use the interference formula for two coherent waves from [15, p. 631] that calculates a total intensity I_{tot} given the intensities I_1, I_2 and their phase difference ϕ over

$$I_{\text{tot}} = I_1 + I_2 + 2\sqrt{I_1 I_2}\cos\phi. \tag{15}$$

As the RCS, respectively the equivalent surface areas, are comparisons of the scattered and received power densities (i.e. their intensities) at a receiver [16, Sec. 11.3], the total RCS σ_{tot} can be formulated as:

$$\begin{aligned}\sigma_{\text{tot}} = \Gamma\sigma_{\triangle} + \frac{2}{3}(1-\alpha)(1-\Gamma)^2\sigma_{\triangle} \\ + 2\sqrt{\Gamma\sigma_{\triangle}\cdot\frac{2}{3}(1-\alpha)(1-\Gamma)^2\sigma_{\triangle}}\cos(2\pi\frac{L\epsilon_{\text{r}}}{\lambda}).\end{aligned} \tag{16}$$

B. Determination of the Loss Coefficient

The unknown loss coefficient α is found by comparing simulation results of the RCS of a conventional corner reflector and a dielectric trihedral one of similar size. The simulation is done with CST Studio Suite using the FIT solver with a linearly polarized plane wave excitation at 77 GHz and a lossless dielectric with $\epsilon_{\text{r}} = 2.47$. The mean difference

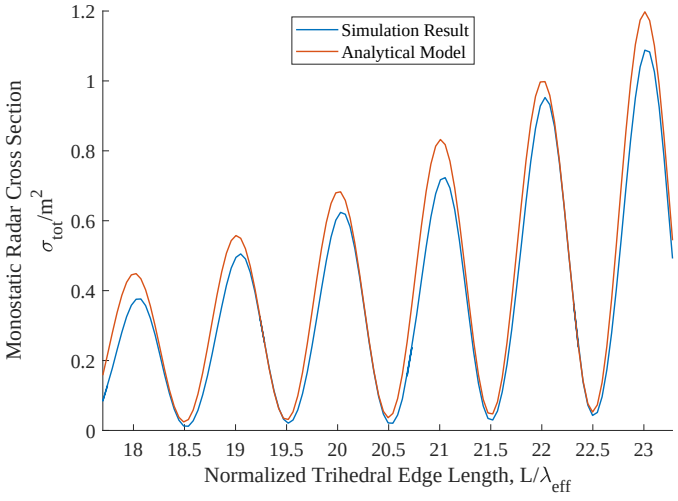

Fig. 6. Comparison of the simulated and calculated RCS. The sinusoidal behavior is in congruence. Only a minuscule deviation of the total RCS is visible. The x-axis is normalized to reflect the electrical size of the corner reflector without giving explicit dimensions, operating wavelengths or material parameters.

of the RCS in a small angular region around perpendicular incidence between the simulated metallic corner reflector and the dielectric trihedral is found to be approximately $-7\,\mathrm{dB}$. This corresponds to an estimated loss coefficient of $\hat{\alpha} = 0.8$. This is in plausible correspondence with the measurement results from Fig. 1 that yield approximate losses of about $-8\,\mathrm{dB}$. As this is only an approximative value it will be used to start the evaluation. This loss coefficient is likely to change suspect to the relative permittivity, i.e. the electrical size of the trihedral. As power loss is occurring at the corners where the isosceles surfaces meet, smaller effective wavelengths will likely lead to less power escaping the total internal reflection.

C. Evaluation of Analytical Model

To evaluate the analytical model, a sweep of the edge length is performed to obtain the RCS as a function of L. Alternatively, a suitable frequency sweep with fixed dimensions or a sweep of the relative permittivity would achieve similar results. The comparison results are presented in Fig. 6. Looking at the oscillatory behavior of the analytical and simulative solution, a correspondence of the respective traces is clear. Small deviations are numerical artifacts of the relatively coarse step size of the length sweep. For destructive interferences the total RCS almost completely vanishes and only rises gradually for larger dimensions. The envelope of the maxima, on the other hand, steadily increases. Overall, the simulation and the analytical model are in good agreement.

V. Conclusion

Dielectric trihedral corner reflectors share similar retroreflective abilities as their metallic counterparts. It is shown that for a trihedral, perpendicular incident rays inside the geometry travel a constant distance independent of their entry point when reflected thrice. The RCS of a dielectric trihedral is analytically derived by comparing the two reflecting surfaces with known RCS values. Perpendicular impinging waves reflected at those surfaces coherently interfere and, depending on the electrical size of the trihedral, constructive or destructive interference occurs. Non dielectric power losses are discussed by comparing the dielectric corner reflector with a conventional one. The analytical model is evaluated and verified exhibiting only a small error margin to FIT RCS simulations.

References

[1] J. R. Wait, "Scattering of a plane wave from a circular dielectric cylinder at oblique incidence," *Canadian journal of physics*, vol. 33, no. 5, pp. 189–195, 1955.

[2] M. Andreasen, "Back-scattering cross section of a thin, dielectric, spherical shell," *IRE Transactions on Antennas and Propagation*, vol. 5, no. 3, pp. 267–270, 1957.

[3] C. Y. Pon and D. J. Angelakos, "Back-scattering from dielectric cones," University of California, Berkeley Electronics Research Lab, Tech. Rep., 1960.

[4] J. J. Stephens, "Radar cross-sections for water and ice spheres," *Journal of the Athmospheric Sciences*, vol. 18, no. 3, pp. 348–359, 1961.

[5] T.-K. Wu, "Radar cross section of arbitrarily shaped bodies of revolution," *Proceedings of the IEEE*, vol. 77, no. 5, pp. 735–740, 1989.

[6] Y.-C. Hou, W.-J. Liao, J. Ke, and Z.-C. Zhang, "Broadband and broad-angle dielectric-loaded RCS reduction structures," *IEEE Transactions on Antennas and Propagation*, vol. 67, pp. 3334–3345, 2019.

[7] T. Beeharry, R. Yahiaoui, K. Selemani, and H. Ouslimani, "A co-polarization broadband radar absorber for RCS reduction," *Materials*, vol. 11, 2018.

[8] S. Xiong, Y. Feng, T. Jiang, and J. Zhao, "Designing retrodirective reflector on a planar surface by transformation optics," *AIP Advances*, vol. 3, no. 012113, pp. 1–7, 2013.

[9] A. Alhaj Abbas, M. El-Absi, A. Abuelhaija, K. Solbach, and T. Kaiser, "Metallic reflectors with notched rcs spectral signature using dielectric resonators," *Electronics Letters*, vol. 56, no. 6, pp. 273–276, 2020.

[10] C. Buchberger, F. Pfeiffer, and E. Biebl, "Dielectric corner reflectors for mmwave applications," *Advances in Radio Science*, vol. 17, no. F., pp. 197–203, 2019.

[11] H. Eckhardt, "Simple model of corner reflector phenomena," *Applied Optics*, vol. 10, no. 7, pp. 1559–1566, 1971.

[12] Texas Instruments, *AWR1642 Evaluation Module (AWR1642BOOST) Single-Chip mmWave Sensing Solution, SWRU508C*, 2020, Available Online: https://www.ti.com/lit/ug/swru508c/swru508c.pdf, Accessed: September 2021.

[13] F. Pfeiffer, E. Biebl, and K.-H. Siedersberger, "Determination of complex permittivity of lrr radome materials using a scalar quasi-optical measurement system," *Advanced Microsystems for Automotive Applications 2008*, p. 205, 2008.

[14] E. F. Knott, *Radar Cross Section Measurements*. Springer Science & Business Media, 1993.

[15] E. Hecht, *Optik*, 5th ed. Oldenburg Wissenschaftsverlag, 2009.

[16] M. Skolnik, *Radar Handbook*, 2nd ed. McGraw-Hill Education, 1990.